Experimental and modeling approach of irradiation defects recovery in zirconium alloys: impact of an applied stress

Joë Ribis, Fabien Onimus, Jean-Luc Béchade, Sylvie Doriot, Chantal Cappelaere, Clément Lemaignan, Alain Barbu, Olivier Rabouille

Ribis, J., Onimus, F., Béchade, J.L., et al., 2009. Experimental and modeling approach of irradiation defects recovery in zirconium alloys: Impact of an applied stress. In Zirconium in the Nuclear Industry: 15th International Symposium. ASTM International, ASTM STP 1505. J. ASTM Int. 5(3), 101118. DOI: 10.1520/STP48162S

Joël Ribis,[1] *Fabien Onimus,*[1] *Jean-Luc Béchade,*[1] *Sylvie Doriot,*[1] *Chantal Cappelaere,*[2] *Clément Lemaignan,*[3] *Alain Barbu,*[4] *and Olivier Rabouille*[2]

Experimental and Modeling Approach of Irradiation Defects Recovery in Zirconium Alloys: Impact of an Applied Stress

ABSTRACT: During neutron irradiation, both interstitial and vacancy loops are formed in high concentration in zirconium alloys. Due to this high density of loops, the material is considerably hardened, but the recovery of the radiation damage during a heat treatment leads to a progressive softening of the irradiated material. The recovery of the radiation induced hardening has been investigated using microhardness tests. Transmission electron microscopy (TEM) observations performed on irradiated foils have also shown that the loop density falls while the loop size increases during the thermal annealing. Furthermore, the TEM analysis has revealed that only vacancy loops are present in the material after long term annealing, the interstitial loops having entirely disappeared. A numerical cluster dynamic modeling has also been used in order to reproduce the material recovery for various annealing conditions. The microstructural evolution during mechanical testing with various loading conditions has also been studied. It has been shown that during a creep test with low applied stress (130 MPa) and high temperature (450°C), the microstructure evolution can essentially be explained by the thermal recovery of the loops leading to glide of dislocations as found for an non-irradiated material. At intermediate temperature (400°C), it is shown that for low stress level (130 MPa) the microstructure evolution can also be explained by the thermal recovery of loops, whereas for higher stress (250 MPa), sweeping of loops by gliding dislocations can also occur. In addition, for an applied stress of 130 MPa and a temperature of 400°C, dislocation density is higher in the irradiated material than in the non-irradiated material deformed in the same conditions. It is also shown that secondary slip systems are more activated in the irradiated material than in the non-irradiated material. From this detailed analysis, the mechanical behavior during creep is interpreted in terms of microscopic deformation mechanisms.

KEYWORDS: zirconium alloys, dislocation loops, annealing, TEM, microhardness, creep

Introduction

Zirconium alloys are commonly used in nuclear pressurized water reactors (PWRs) as fuel rod cladding tubes. However, the effect of the annealing of radiation damage during a heat treatment on the material properties is not clearly understood. It is well known that, at the microscopic scale, neutron irradiation induces a high density of small dislocation loops. These loops are induced by the agglomeration and the collapse of interstitial and vacancy point defects. In zirconium alloys, two types of loops coexist in the material: interstitial and vacancy loops. Their Bürgers vector is $\vec{b}=\langle 11\bar{2}0\rangle$, and their habit plane is close to the plane $\{10\bar{1}0\}$ [1,2]. It has to be pointed out that the reason for the coexistence of the two types of loops may be due to the anisotropic diffusion of interstitial defects in the hcp (hexagonal close packed) lattice, but is not yet clearly understood [3]. After irradiation at 320°C during five PWR cycles (corresponding to a fluence of 11×10^{25} n·m^{-2}) the microstructure of the material contains a very high density of small dislocation loops. This is illustrated by Fig. 3a, showing the 5 PWR cycles as-irradiated material microstructure.

The high density of dislocation loops has a strong effect on the mechanical behavior of the material. Indeed, due to a strong interaction between dislocations and loops [4], the material is considerably hard-

[1] CEA-DEN/DANS, DMN/SRMA, CEA/Saclay, 91191 Gif-sur-Yvette Cedex, France. Corresponding author, electronic mail: joel.ribis@cea.fr
[2] CEA-DEN/DANS, DMN/SEMI, CEA/Saclay, 91191 Gif-sur-Yvette Cedex, France.
[3] CEA-DEC, Dir, CEA/Grenoble, 38054 Grenoble Cedex, France.
[4] CEA-DEN/DANS, DMN/SRMP CEA/Saclay, 91191 Gif-sur-Yvette Cedex, France.

ened by the irradiation [5]. Consequently, the yield stress of the irradiated material is higher than the yield stress of the non-irradiated one [6]. Nevertheless, this radiation damage can be recovered by a thermal annealing at a higher temperature than the irradiation temperature [7,8].

One of the possible recovery mechanisms of loops implies exchange of vacancies in the bulk material [9]. Indeed, due to the high formation energy of interstitials, no interstitials can appear in the material without irradiation. According to this process, vacancy loops can grow by absorbing vacancies and shrink by emitting vacancies while the interstitial loops can grow and shrink from the opposite processes. With such a mechanism, large loops will grow at the expense of the small ones. Consequently, at the end of a thermal heat treatment, the microstructure will be composed of large loops but with a low density.

During the mechanical testing, the microstructure of irradiated zirconium alloys also evolves. Indeed, it has been shown that clearing of loops occurs by the dislocation channeling mechanism during mechanical tests performed on recrystallized and neutron irradiated zirconium alloys. It has been recently established that for transverse tensile tests and internal pressure tests, only basal channels can be observed, up to the uniform elongation [10]. The loop clearing by the glide of the dislocations and the thermal annealing of loops can therefore have a strong impact on mechanical properties, especially in the conditions of a creep test, depending on the loading conditions (temperature and stress level).

The aim of the present study is first to analyze the recovery of loops during a thermal anneal, and in particular to determine the phenomenon kinetics and the activation energy. Since the loops harden the material, an experimental technique used to characterize the microstructure recovery is microhardness testing. Microstructure observations are also carried out by TEM. The microhardness tests allow access to the recovery kinetics, while the TEM observations give a fine characterization of the microstructure: the nature of loops, size, and density.

A cluster dynamic modeling is then used to reproduce the microstructure and the microhardness evolution.

The microstructure evolution during various creep tests has also been studied in detail. The results are compared to pure thermal annealing and the mechanical behavior of the material is discussed in terms of microscopic deformation mechanisms observed by TEM. The aim of this analysis is first to understand the effect of an applied stress on recovery of loops, and second to clarify what are the glide system modifications due to the presence of loops. Then both results are used to interpret the creep behavior by referring to the results obtained on the pure thermal annealing and the one obtained after creep tests.

Materials and Experimental Details

The materials studied were a recrystallized annealed zirconium alloy Zr-1 %Nb-O and a stress relieved Zircaloy-4. Due to the fabrication process and the hcp zirconium anisotropy, cladding tubes of zirconium alloys are strongly textured. The $\langle c \rangle$ axis is close to the radial direction [11]. The materials studied were irradiated at 320–350 °C in a PWR up to fluences (>1 MeV) between 9×10^{25} and 11×10^{25} n·m^{-2} (4 and 5 PWR cycles). The Vickers microhardness experiments were carried out with 200 g load along the z-direction of the tube (on the r-θ section of the tube). To provide correct statistical results, about ten hardness measures were performed for each sample at room temperature. The samples were mechanically polished and indented in a hot cell.

TEM observations were performed on a Philips EM 430 microscope at 300 kV. The thin foils were mechanically thinned in hot cells and then electropolished in glove box.

The annealing conditions for samples studied by microhardness and TEM observations are given in Table 1.

The mechanical tests were performed on Zr-1 %Nb-O samples with internal pressure loading at temperatures ranging from 350 °C up to 450 °C. Five irradiated and non-irradiated creep-tested specimens were studied. All irradiated tests were performed in hot cells. The mechanical tests conditions are given in Table 2.

The samples were cladding tubes with an external diameter of 9.5 mm and a wall thickness of 0.57 mm. The samples were gripped at one end to the gas circuit with a Swagelock system. They were closed at the other end by a second Swagelock system. Once the temperature was stabilized, the sample was pressurized with argon in order to reach the set stress. Before the test, the sample diameter and

TABLE 1—*Annealing conditions for microhardness tests and TEM observations. (a) Zr1 %Nb-O. (b) Stress relieved Zircaloy-4 (4 PWR cycles).*

(a)				
Annealing time, h	Annealing temperature, (°C)			Stress, MPa
As-irradiated	—	—	—	—
50	350	400	—	—
100	350	400	—	—
240	—	400[a]	—	130
250	350[a]	400[a]	—	—
500	350[a]	400[a]	—	—
720	—	—	450[a]	130
960	—	—	450[a]	—
(b)				
As-irradiated	—	—	—	
500	—	380	400	
1500	350	380	400	
3000	350	380	400	

[a]TEM observations.

thickness were accurately controlled. The sample external diameter elongations were measured by two opposite displacement transducers located at the middle of the sample.

Microstructure Evolution During Thermal Annealing

Microhardness Tests Analysis

—Microhardness results for the Zr-1 %Nb-O and for the stress relieved Zircaloy-4 are presented in Table 3 and Fig. 1.

It can be noticed in Table 3 that the initial irradiation hardening value, obtained for the Zr-1 % Nb-O samples, is equal to: $\Delta H_v = 76\ \mathrm{kg \cdot mm^{-2}}$. This value is close to the value obtained by Nakatsuka [12] and Adamson [8] for the Zircaloy-2 material. Indeed, after an irradiation of about $2.8 \times 10^{25}\ \mathrm{n \cdot m^{-2}}$ (1 PWR cycle), Nakatsuka obtains a hardness increment of $80\ \mathrm{kg \cdot mm^{-2}}$, and Adamson obtains the same microhardness value after an irradiation at a fluence of $6.5 \times 10^{24}\ \mathrm{n \cdot m^{-2}}$ (<1 PWR cycle). It can also be noticed that the recovery kinetics increases with temperature. This fact shows the thermal activated character of the phenomenon. It can be observed in Fig. 1 that the recovery is relatively fast for both Zr-1 % Nb-O and Zircaloy-4. For instance, at 400°C after 500 h, more than 70 % of the Zr-1 % Nb-O initial hardening was recovered. Beyond 500 h, the Zr-1% Nb-O material continued recovering progressively its microhardness towards its non-irradiated value. However, the irradiation-enhanced precipitates (that is to say, the β-Nb precipitates) were not dissolved during the thermal annealing and may still harden the material. However, the anneal time is not long enough to clearly prove this point. This precipitation phenomenon does not exist for the Zircaloy-4 alloy. By consequence, the microhardness continues to decrease towards its initial state. In addition the hardness can decrease beyond its initial state if recrystallization and/or recovery of the dislocation network occurs as it is shown by Dunlop [13]. It has to be noticed that no recrystallization

TABLE 2—*Creep tests performed on Zr-1 %Nb-O irradiated samples.*

Temperature, °C	Applied stress, MPa	Test time, h	Irradiation
450	130	720	4 PWR cycles
450	130	95	Non-irradiated
400	130	240	5 PWR cycles
400	130	72	Non-irradiated
400	250	83	4 PWR cycles
350	300	500	4 PWR cycles [10]

TABLE 3—*Microhardness results at room temperature for (a) Zr-1 %Nb-O alloy (4 PWR cycles irradiated at 350°C) and for (b) stress relieved Zircaloy-4(4 PWR cycles irradiated at 350°C)*

(a)

Annealing time, h	Hardness ($kg \cdot mm^{-2}$)		
	350°C	400°C	450°C
Non-irradiated	161	161	161
As-irradiated	237	237	237
50	229	209	—
100	224	205	—
250	209	190	—
500	199	184	—
720	—	—	177
960	—	—	182

(b)

Annealing time, h	Hardness ($kg \cdot mm^{-2}$)		
	350°C	380°C	400°C
Non-irradiated	224	244	244
As-irradiated	301	301	301
500	—	260	249
1500	263	258	246
3000	252	242	237

occurred during the tests presented here.

If we compare the annealing behavior of the Zr-1 % Nb-O alloy and the stress relieved Zircaloy-4, the first difference noticed concerns the phenomenon kinetics. Indeed, at 400°C, after 500 h, 91 % of the irradiated microstructure is recovered for the stress relieved Zircaloy-4, whereas for the same time and temperature, only 70 % is recovered for the Zr-1 % Nb-O alloy. However, this analysis has to be moderated since both materials undergo a decrease of hardness of 50 $kg \cdot mm^{-2}$ after 500 h at 400°C, the initial hardness of the Zircaloy-4 being higher than the initial hardness of the irradiated Zr-1 % Nb-O alloy due

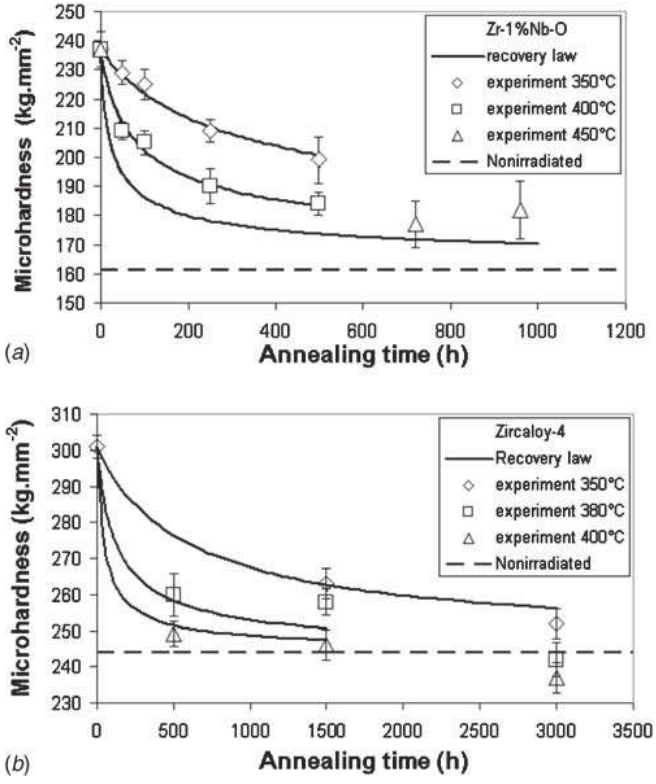

FIG. 1—*Comparison between experimental results and the recovery law identification.*

to the initial dislocation network. The dislocation network can also recover at the same time as the dislocation loops recover, contributing to a more important softening of the material. The initial dislocation network can also have an impact on the irradiation annealing of the stress relieved Zircaloy-4. These initial dislocations can indeed be considered as source or sink of vacancies. In addition, the niobium could also stabilize the irradiation defects [14].

Hardness Recovery Empirical Law

Microhardness data can be used to adjust an empirical law allowing to describe the kinetics of the recovery [15].

The recovered fraction of hardness f can be defined as

$$f = \frac{H_v^{AsI} - H_v(t)}{H_v^{AsI} - H_v^{NI}}$$

H_v^{AsI} is the as-irradiated material hardness, H_v^{NI} is the non-irradiated material hardness and $H_v(t)$ is the current hardness of the material all along the thermal annealing. The remaining fraction of irradiation hardening is, therefore, $1-f$.

According to Dollins [16], this hardness recovered fraction follows a chemical kinetics empirical law, expressed as:

$$\frac{df}{dt} = k(1-f)^n \tag{1}$$

where $k=k_0e^{-Q/kT}$. The three parameters k_0, Q, and n have been adjusted to experimental results obtained at 350°C and 400°C for the Zr-1 %Nb-O alloy and the stress relieved Zircaloy-4. Because the recovery of the dislocation network and the recovery of the dislocation loops have different activation energies, it would be appropriate to consider these two phenomena separately. This analysis is confirmed by the work of Dunlop [13]. Indeed, it was shown in [13] that during 10 000 hours at 400°C, the yield stress of the non-irradiated stress relieved material only decreased by 25 %, which showed the slow recovery rate of the dislocation network. In a first approximation, the reference microhardness ($H_v^{NI}=244$) of the stress relieved Zircaloy-4 is taken as the hardness of the non-irradiated stress relieved Zircaloy-4. This neglects the fact that the hardness can decrease beyond its non-irradiated value due to the recovery of the dislocation network and the recrystallization. Consequently, only the points with microhardness values higher than the stress relieved non-irradiated value were considered for the fitting procedure. The values found for the three parameters of the empirical law for the Zr-1 %Nb-O alloy are $n=3.1$, $k_0=3.8\times10^2$ s^{-1}, and $Q=1.1$ eV. In the case of the stress relieved Zircaloy-4, the values obtained are $n=2.3$, $k_0=1.8\times10^8$ s^{-1}, and $Q=1.8$ eV. Despite the disparity between k_0 for the Zr-1 %Nb-O alloy and the stress relieved Zircaloy-4, the value $k=k_0e^{-Q/kT}$, is similar for the two materials and close to 2×10^{-6} s^{-1} at 400°C. The exponent value n ($n=3.1$ for the Zr-1 %Nb-O alloy and $n=2.3$ for the stress relieved Zircaloy-4) are compatible with Dollins results [16]. The activation energies obtained for the Zr-1 %Nb-O alloy ($Q=1.1$ eV) differs from the value given by Torimaru [15] and Dollins [16], on the order of 2 eV, using 1-h heat treatments on irradiated recrystallized Zircaloy-2. Douglass [17] reviews self-diffusion results from various authors where the activation energies are found between 1 eV and 2.3 eV. According to Dollins and Torimaru [15,16], if the activation energy found is close to those corresponding to the self-diffusion, the possible mechanism controlling the recovery is the vacancy exchange between the loops. Nevertheless, other mechanisms could occur and also lead to loop growth, such as coalescence after loop gliding [18].

This empirical law enables one to reproduce correctly the recovery experimental results for both the Zr-1 %Nb-O alloy and the stress relieved Zircaloy-4 (Fig. 1). It has to be noticed that there is a lack of experimental points, especially at the beginning of the thermal annealing, to reproduce correctly the recovery of the stress relieved Zircaloy-4.

TABLE 4—*Size and density of loops for various annealing conditions.*

Annealing temperature, °C	Stress, MPa	Annealing time, h	$\langle d \rangle$, nm	N, (m^{-3})
—	—	0	15.6	1.2×10^{22}
350	—	250	17	3.2×10^{21}
350	—	500	20.3	3.3×10^{21}
400	—	250	18.2	2.5×10^{21}
400	—	500	24.5	10^{21}
450	130	720	139	6×10^{19}
450	—	960	176	1.2×10^{22}

Transmission Electron Microscopy Observations

Evolution of Size and Density of Loops During Thermal Annealing

The size and density evolution during the thermal annealing were studied quantitatively by TEM. Due to the high initial dislocation density inside the Zircaloy-4 material, the loops' microstructure can not be studied by TEM on Zircaloy-4. Consequently, only the Zr-1 %Nb-O alloy was studied by TEM. Table 4 provides the results obtained showing the evolution of the size and density of loops as a function of thermal annealing conditions (the thin foil's thickness has been estimated to a value of 150 nm ±50 nm by stereographic measurements).

Table 4 presents the density of loops (N) and their average diameters ($\langle d \rangle$) for various annealing times and temperatures. The histograms presented in Fig. 2 show the distribution of size of the loops. It can be noticed that the loops' size increases and the density decreases during the thermal annealing.

The histogram corresponding to the as-irradiated material has the best statistical distribution because of the high loop density. The distribution of the as-irradiated loops ranges from 4 nm up to 38 nm. The average loop diameter is a little larger than the one presented by Kelly and Blake [19]. the difference could be explained by the counting difficulty. The small objects, with diameter less than 4 nm, cannot be observed by TEM, but only by small angle neutron scattering, as reported in [20].

The histogram obtained after thermal annealing at 350°C during 250 h and 500 h (Figs. 2(*b*) and 2(*c*))) shows a slight evolution of loops compared to the as-irradiated material. The density of loops is still high and the diameter still small.

On the other hand, for a 400°C thermal anneal of 250 h (Fig. 2(*d*)), the majority of the loops shrunk while the other ones have grown.

For the samples annealed at 450°C for 720 h and 960 h (Fig. 2(*e*) and 2(*f*))), the TEM observations prove that the loops have a large size (>100 nm) and a low density.

From these histograms it can be concluded that the irradiation microstructure recovery occurs by loop growth and density decrease. The TEM micrographs in Fig. 3 illustrate the size of loops and density evolution during the thermal annealing.

Loop Nature Determination

As both interstitial and vacancy dislocation loops are present in the material, it is important to analyze how the two types of loops evolve during a thermal annealing that is essentially controlled by exchange of vacancies. The evolution of the nature of loops has been studied during thermal annealing by the outside/inside contrast method using TEM [21]. Depending on the habit plane of loops, the Bürgers vector, and the diffraction vector $\vec{g}$, the studied loop presents a different contrast as a function of its nature (Fig. 4). The zone axis used for this study is $B=\langle 11\bar{2}3 \rangle$ and the diffraction vector used is $\vec{g}=\langle 1\bar{2}1\bar{2} \rangle$. Due to the orientation of this diffraction vector, only the orientation of the loops relative to this vector is needed to determinate the loop nature [21].

To illustrate this method, Fig. 4 shows a loop presenting an outside contrast (Fig. 4(*a*)) with $+g$ diffraction vector and an inside contrast (Fig. 4(*b*)) with $-g$ diffraction vector. The deviation vector used is negative and the orientation of the loop compared to the diffraction vector ($+g$) is such that $+\vec{g}.\vec{n}>0$

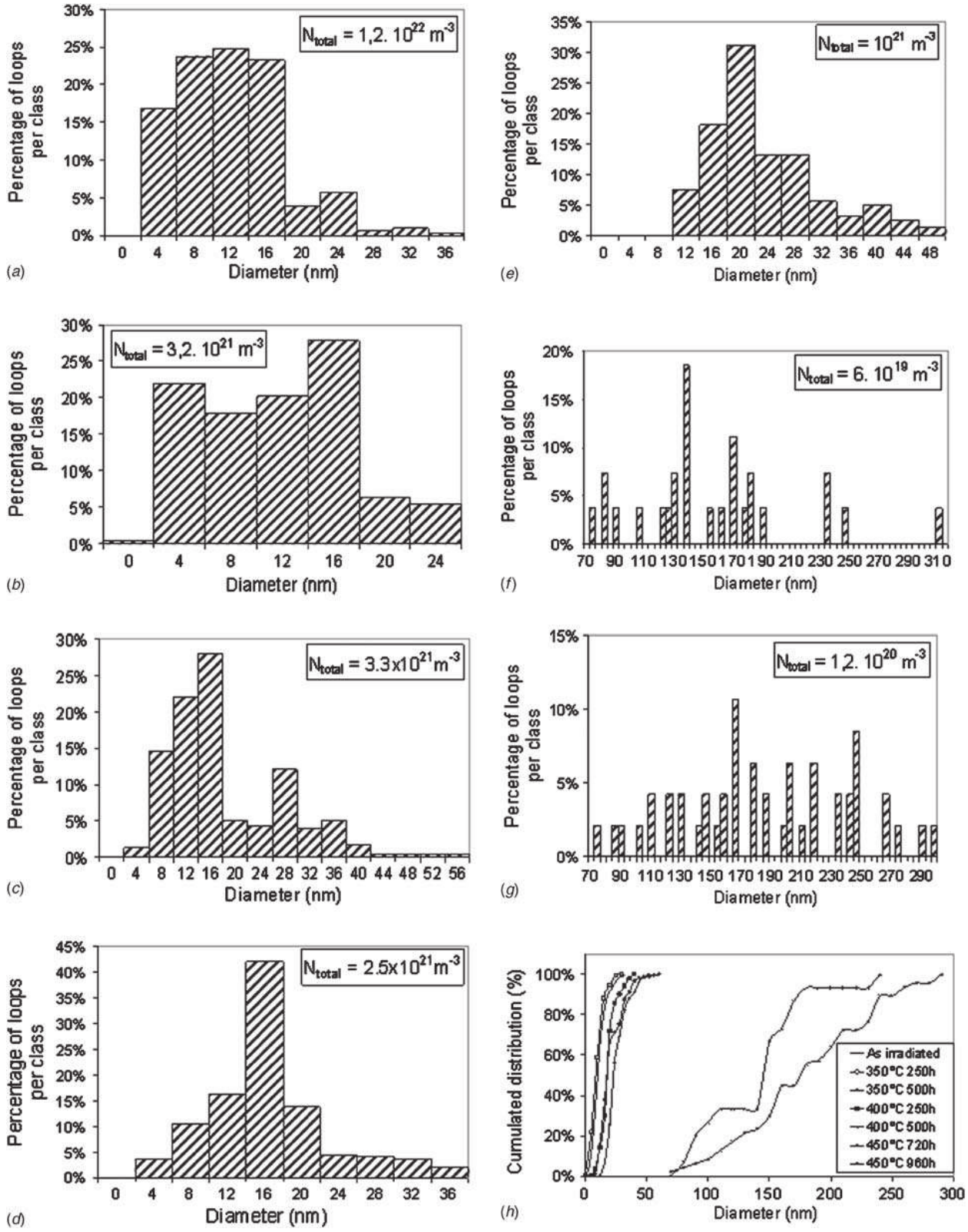

FIG. 2—*Various annealing conditions histograms: (a) as-irradiated, (b) 250 h at 350°C, (c) 500 h at 350°C, (d) 250 h at 400°C, (e) 500 h at 400°C,(f) 720 h at 450°C (130 MPa), (g) 960 h at 450°C, (h) Cumulated distribution of loop diameters.*

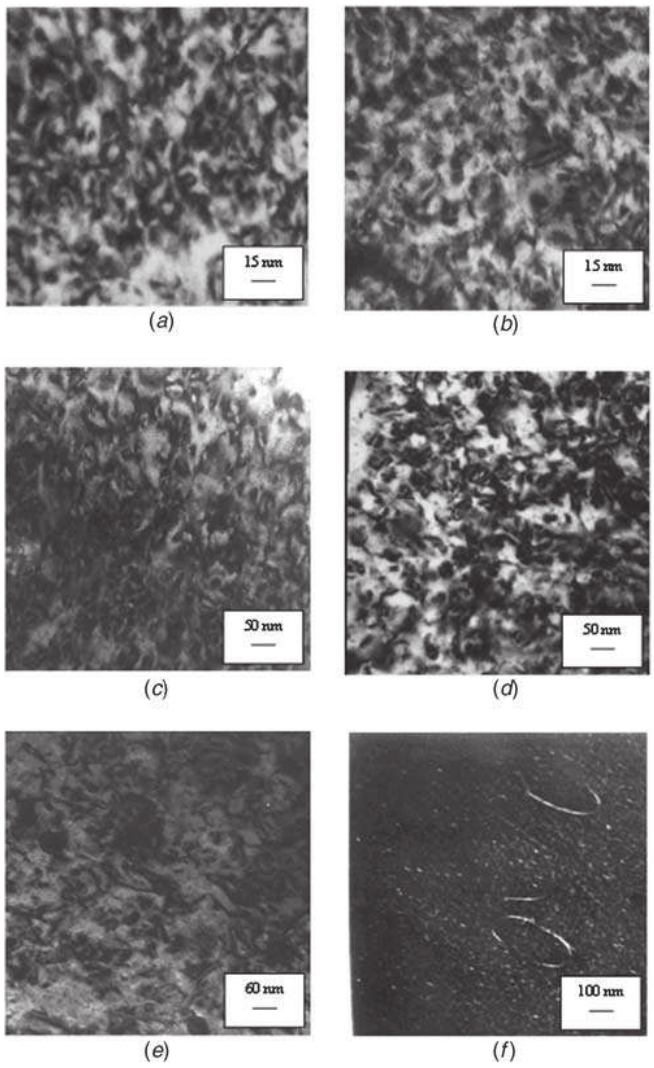

FIG. 3—*Microstructure (a) as-irradiated (bright field) and (b) 250 h at 350°C (bright field).*

(Fig. 5), where $\vec{n}$ is the normal of the habit plan of loops (here, $\vec{n}=\langle 1\bar{1}00\rangle$). With such an orientation, the loop presents an outside contrast when it is imaged with $+g$ and $s<0$, with s the Bragg deviation parameter, which means that the loop is vacancy type according to Table 5.

No nature determination has been carried out on the as-irradiated sample because of the high density of loops and the observation difficulty entailed. However, according to the data in the literature, roughly 50 % of the loops present in the material are interstitial loops and 50 % are vacancy loops [19].

After a thermal annealing of 250 h at 350°C, the evolution of loops was not important and the microstructure was similar to the as-irradiated microstructure. The microstructure is still composed of 50 % interstitial loops and 50 % vacancy loops. The same result was observed for the sample annealed at 350°C for 500 h (see Table 6).

After an annealing of 250 h at 400°C, a predominance of vacancy loops over interstitial loops during the thermal annealing was observed. This tendency was confirmed by the observations performed on the sample annealed at 450°C during 960 h, where the microstructure was composed of vacancy loops only.

These results are in agreement with the results presented by Kelly and Blake [19], showing that the interstitial loops disappear during annealing. It can be concluded that the interstitial and vacancy loops do not evolve during annealing in a similar way. The interstitial loops recover faster than the vacancy ones and only large vacancy loops remain.

Microhardness Prediction from TEM Microstructural Analysis

A simple irradiation hardening model [22,23] shows that the critical resolved shear stress (τ) of the material increases during irradiation by an increment $\Delta\tau$, which can be expressed as:

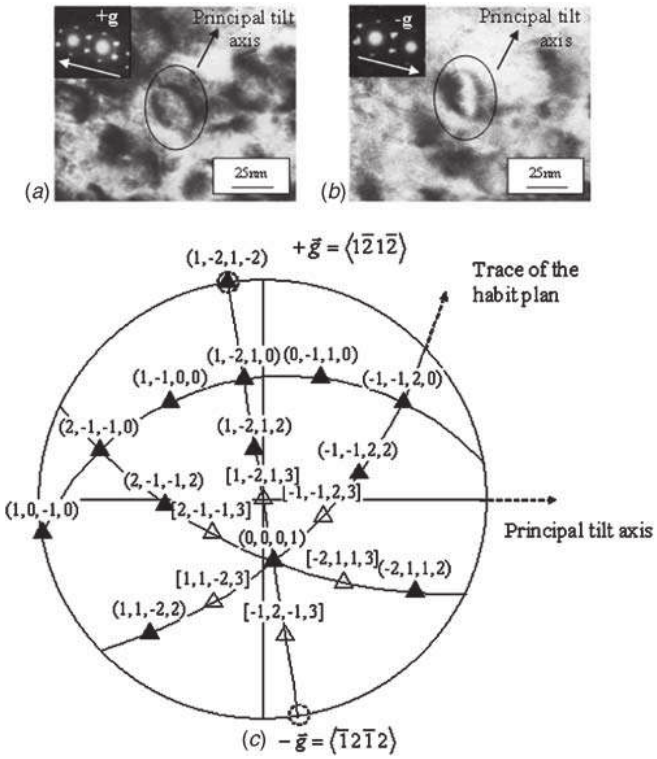

FIG. 4—*Loop contrast: (a) outside contrast (+g, s<0), (b) inside contrast (−g, s<0), (c) stereographic projection* $+\vec{g} = \langle 1\bar{2}1\bar{2} \rangle$.

$$\Delta\tau = \alpha\mu b\sqrt{Nd} \tag{2}$$

where α is the obstacle force, μ is the shear modulus, b is the Bürgers vector, N is the density of loops, and d is their mean diameter. Furthermore, it is known that a proportional relation exists between the yield stress and the Vickers hardness [24]. The hardness increment can be expressed as the following expression [25,26]:

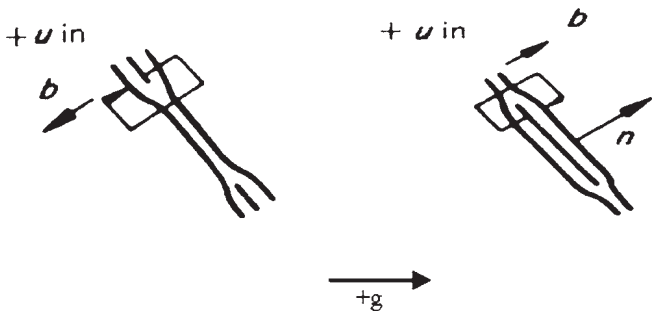

FIG. 5—*Vacancy and interstitial loop orientation compare to the diffraction vector.*

TABLE 5—*Loop contrast versus g and s and the orientation of the habit plane.*

		Loop contrast	
$s>0$	$+g$	Intern	Extern
	$-g$	Extern	Intern
$s<0$	$+g$	Extern	Intern
	$-g$	Intern	Extern
	Type	Vacancy	Interstitial

TABLE 6—*Loops, nature evolution as a function of the annealing conditions.*

Annealing time, h	Annealing temperature, (°C)	Percentage of vacancy loops %	Number of loops analyzed
As-irradiated	—	50 [19]	—
250	350	50	19
500	350	50	24
250	400	65	37
500	400	71	38
960	450	100	13

$$\Delta Hv = CM\alpha\mu b\sqrt{Nd} \tag{3}$$

where M is the Taylor factor and C is the proportionality coefficient between the yield stress and the hardness (from the yield stress of non-irradiated stress relieved Zircaloy-4 given by Dunlop [13], this C coefficient is estimated at 0.3, which is in good agreement with the literature [27]).

The N and d values provided by the microscopy investigations are used to plot the hardness increment ΔH_v as a function of $\sqrt{Nd}$.

As seen in Fig. 6, the hardness increment varies linearly with the root of the product of the density and the diameter of loops. The numerical value of $CM\alpha\mu b$ is equal to 5.8×10^{-9} kg.mm^{-1}, this value is in good agreement with the value calculated from the results of Adamson [8], which is 5×10^{-9} kg.mm^{-1}. The different coefficients composing $CM\alpha\mu b$ are $C=0.3$ and $\mu=3.6\times10^4$ MPa at room temperature [28] and b=3.232 Å. Therefore, the value of $M\alpha$ is equal to 1.7. Considering that M lies between 2 [29] and 4 [30], a value for α is obtained between 0.4 and 0.8, which is in agreement with the literature data [26] for the strength of this obstacle for dislocation glide.

This correlation gives a precious link between the microscopic scale and the macroscopic scale, which can be used to predict the mechanical properties of the material from the microstructure evolution.

Discussion on the Recovery Mechanism

Based on the TEM observations, a recovery mechanism of loops can be proposed. It is first considered that due to the high formation energy of interstitials, only vacancy exchange controls the recovery of loops. It can be derived that variation in energy of a vacancy loop when absorbing a vacancy point defect is $E_v=\tau b^2/r$. In addition, it can be also shown that the variation in energy of an interstitial loop when absorbing a vacancy point defect is $E_v=-\tau b^2/r$, where τ is the line tension, r the radius of loops, and b the Bürgers vector modulus. It is assumed that the formation energy of vacancies surrounding the loops is $E_v^{bulk}=kT\ln(c_v/c_0)$, where c_0 is the thermal equilibrium vacancy concentration in the material bulk. Consequently, there is a vacancy concentration $c_v^{vl}=c_0e^{\tau b^2/rkT}$ $(c_v^{vl}>c_0)$ around the vacancy loops, and a vacancy concentration $c_v^{il}=c_0e^{-\tau b^2/rkT}$ $(c_v^{il}<c_0)$ around the interstitial loops. In addition, it can be seen that the vacancy concentration at the vicinity of the grain boundaries is equal to the thermal equilibrium vacancy concentration in the material bulk.

Due to the vacancy gradient, a vacancy flux is created from vacancy loops to the grain boundaries, which act as sinks for vacancies, leading to the disappearance of vacancy loops. Another vacancy flux is

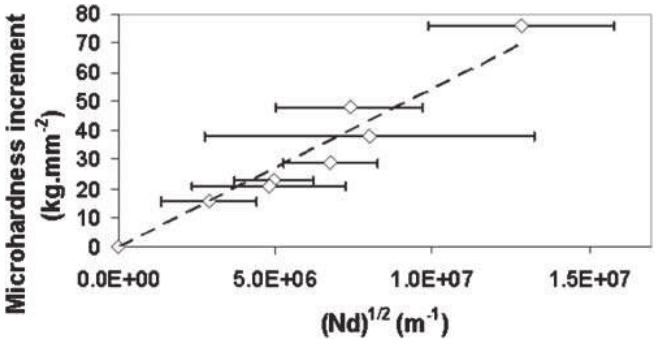

FIG. 6—*Microhardness increment evolution in function of* $(Nd)^{1/2}$.

created from vacancy loops to the interstitial loops ($c_v^{il} < c_v^{vl}$) leading to the disappearance of both vacancy and interstitial loops. A last vacancy flux occurs from the grain boundaries (c_0), which act as sources for vacancies, to the interstitial loops ($c_v^{il} < c_0$) leading to the disappearance of interstitial loops. In addition, since the vacancy concentration around a vacancy loop is expressed as $c_v^{vl} = c_0 e^{\tau b^2/rkT}$, the vacancy concentration is higher for small vacancy loops than for large vacancy loops ($c_v^{vl}(r_1) > c_v^{vl}(r_2) r_1 < r_2$). This concentration gradient also induces a vacancy flux from smaller vacancy loops to large vacancy loops. Consequently, the biggest vacancy loops grow at the expense of the small ones. For this reason, at the same time that interstitial and small vacancy loops disappear, the biggest vacancy loops grow.

Numerical Modeling of the Recovery of Loops

To simulate and predict the evolution of the microstructure during thermal annealing, a numerical modeling has been used. This modeling is based on the homogeneous rate theory applied to cluster dynamics. The modeling has been developed by Duparc et al. [31] and applied to zirconium alloys by Christien et al. [32] to simulate electron irradiation.

Model Description

In material science, cluster dynamics is based on kinetic equations describing the formation and evolution of clusters of solute atoms or point defects such as vacancies or self-interstitial atoms (SIAs). It is a very efficient method in term of computational cost. This efficiency is due to a drawback coming from the basic hypothesis of uniform distributions of clusters: the real system is replaced by an effective medium in which all processes occur continuously in time and space. The spatial correlations between clusters are consequently not considered explicitly. In these models, the system is seen as a gas of clusters made of monomers that can be solute atoms, vacancies, or self-interstitial atoms. A consequence is that the total volume fraction occupied by the clusters must be small. The evolution of the number density of clusters of each size n and of a certain kind is treated within the framework of the chemical rate theory. In the most general case, i.e,. when some species are non-conservative, it is described by a set of differential equations of the form:

$$\frac{dC_n}{dt} = \sum_m J_{m \to n} - \sum_q J_{n \to q} + G_n - K_n C_n \tag{4}$$

where C_n is the cluster density of size n and $J_{m \to n}$ the cluster flux from the class of size m to the class n. It is given by:

$$J_{m \to n} = \sum_m w_{m \to n} C_m \tag{5}$$

Putting 5 in 4, we have:

$$\frac{dC_n}{dt} = G_n + \sum_m w_{m \to n} C_m - \sum_q w_{n \to q} C_n - K_n C_n \tag{6}$$

with $w_{m \to n}$ the transition rate per unit concentration from the class of size m to the class of size n. This transition rate includes physical parameters such as the formation energy, migration energy, and emission and absorption energy of clusters.

K_n, which is the loss of clusters of size n at some fixed sinks such as dislocations, grain boundaries, or surfaces, must only be taken into account in the case of non-conservative species as vacancies or SIAs. G_n is the production rate of clusters of size n. This production rate takes into account the creation of point defects and point defects clusters inside displacements cascade under irradiation. By choosing $G_n = 0$, $\forall n$, the recovery of loops during thermal annealing can be computed using this cluster dynamic modeling. A detailed description of the differential equations is given in [31,32]. In the annealing case, due to the impossibility of interstitial formation, the interstitial diffusion is very low in the modeling. In addition, because only interstitial point defects undergo anisotropic diffusion during thermal annealing, only isotropic diffusion occurs.

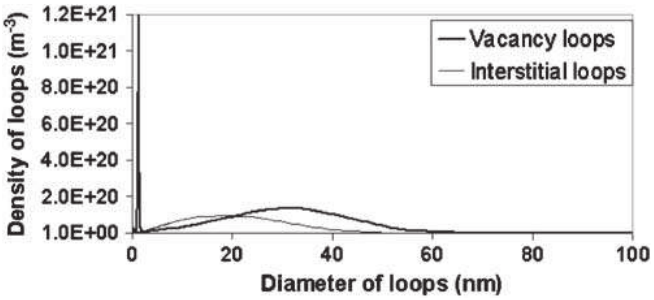

FIG. 7—*Initial distribution of vacancy and interstitial clusters.*

Initial Microstructure

The initial microstructure is taken as the as-irradiated microstructure. Since small point defect clusters cannot be observed by TEM, it is chosen to use a simulated microstructure. This microstructure is obtained by using the model described in [32] which can compute the evolution of point defect clusters under irradiation. This step is not described here. It can be seen in Fig. 7 that the as-irradiated microstructure is similar to the experimental microstructure. Indeed, the microstructure is composed 49 % of interstitial loops and 51 % of vacancy loops. The initial loop density is 1.16×10^{22} m^{-3} for an initial average diameter of 20 nm. Objects of less than 2 nm in size, invisible by electron microscopy, are not taken into account. It can be seen in Fig. 7 that a peak of small vacancy cluster is created due to the production rate of clusters chosen in order to reproduce the formation of vacancy clusters in the middle of the displacements cascade.

Adjustment of the Modeling

The main model coefficients are given in Table 7.

The TEM observations have shown that the size of grains is about 10 μm. The migration energy value is chosen equal to the activation energy provided by the literature: E_{mV}=0.6 eV [33]. The adjustable coefficient is the diffusion pre-exponential coefficient (D_{0V}). The identification of this coefficient is determined for a temperature of 400°C. The other coefficients are chosen equal to those adopted by Christien et al. [32].

The diffusion coefficient obtained is $5 \times 10^{-2} \exp(-0.6\text{eV}/kT)$. This diffusion coefficient value is close to the experimental self-diffusion coefficient [17,34].

Results of the Dynamic Clusters Modeling

Figure 8 represents the density and size evolution of loops during the thermal annealing. This evolution is compared to the experimental points obtained by TEM analysis.

The densities of loops obtained by simulation are close to experimental values when uncertainties are taken into account. Concerning the diameter, the values are a little different from the experimental values, particularly for a temperature of 450°C. Other experimental data and a better adjustment would be necessary to improve the diameter modeling.

Another tendency is confirmed by the model: the vacancy loops dominate over the interstitial loops during the annealing. Indeed, at 450°C at the end of 5 h the interstitial loops have entirely disappeared from the annealed material, as shown in Fig. 9.

TABLE 7—*Main dynamic cluster model input coefficient.*

	Symbol	Value	Ref.
Grain size	d_g	10 μm	
Vacancies formation energy	E_{fv}	1.8 eV	[33]
Vacancies migration energy	E_{mV}	0.6 eV	
Diffusion pre-exponential coefficient	D_{0V}	5×10^{-2} ms^{-2}	[32]

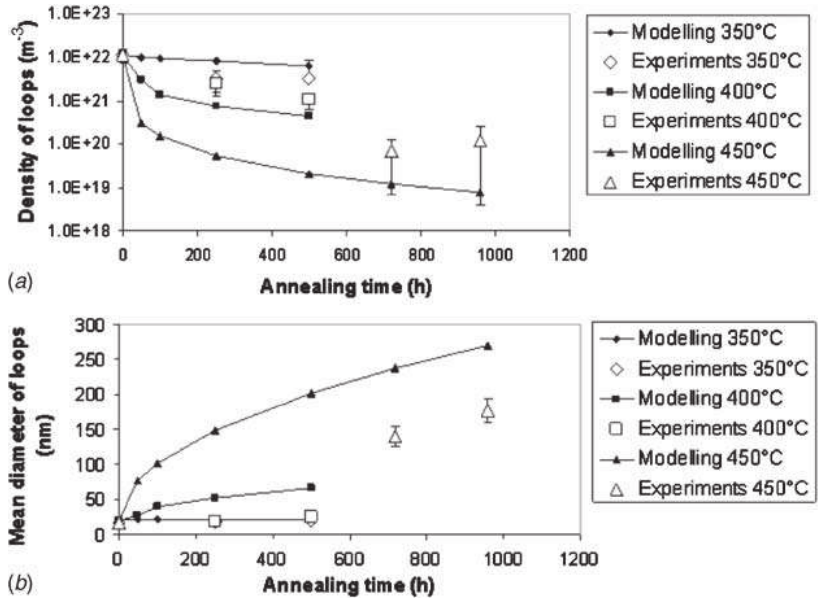

FIG. 8—*Size, density evolution loops according to the model evolution compared to experiments. (a) loops density and (b) average loops diameter.*

Microhardness Evolution According to the Model

Using the irradiation hardening model, it is possible, with a combination of the loop diameter and density computed by the dynamic cluster modeling, to estimate the microhardness evolution during the thermal annealing. The coefficient $CM\alpha\mu b$ is taken at the value of 5.8 10^{-9} kg·mm^{-1}, obtained previously.

The recovery evolution at 400°C and at 450°C, presented in Fig. 10, is well reproduced by the model

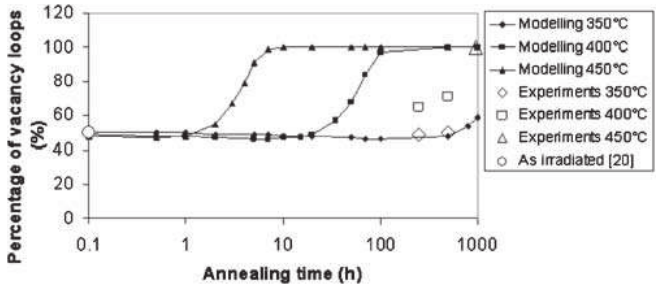

FIG. 9—*Evolution of vacancy loops during a 350, 400, and 450°C thermal annealing.*

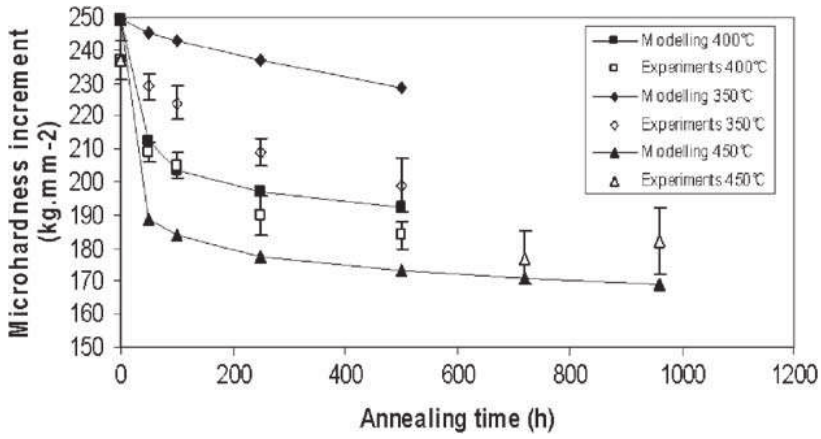

FIG. 10—*Comparative graphs between the microhardness obtained by simulation and experimental microhardness.*

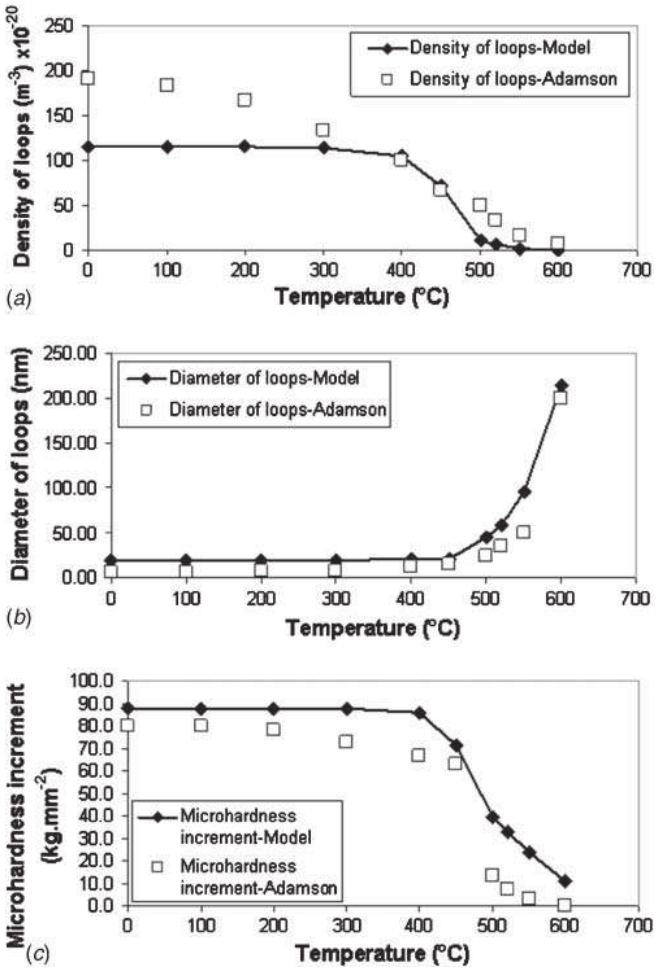

FIG. 11—*Comparison between the results of Adamson and the results of the dynamic clusters model: (a) density, (b) size, and (c) microhardness.*

when experimental uncertainties are taken into account. However, the recovery evolution at 350°C obtained by simulation is different from the experimental values.

The model of dynamic clusters, based on physical law, enables one to extrapolate the microhardness at higher annealing times. However, this model presents a high sensitivity to the input microstructure. Therefore, this input microstructure has to be carefully chosen.

Cluster Model Validation

To validate the numerical cluster model, a comparison between a study performed by Adamson [8] and the results provided by the modeling has been carried out. Indeed, Adamson was among the first workers to highlight the thermal recovery of the irradiation defects in Zircaloys. His work consisted in heating Zircaloy-2 samples that had been irradiated up to a fluence of 6.5×10^{24} n·m^{-2} for 1 h at temperatures of 100, 200, 300, 400, 500, and 600°C. Figure 11 shows the comparison between the results of Adamson and the results of the dynamic clusters model.

As seen in the Fig. 11, the dynamic cluster model is in good agreement with the results of Adamson. The density, diameter, and hardness values are similar and the tendency of the recovery process is correctly reproduced by the cluster model as well. From this comparison, we conclude that the proposed dynamic cluster model is validated.

Microstructure Evolution During Mechanical Testing

In the last part of this paper, the effect of an applied stress during creep testing on the microstructure evolution is studied. From TEM observations, deformation mechanisms are analyzed, leading to a better understanding of the mechanical behavior of the irradiated material.

TABLE 8—*Results for materials annealed without external load (Unstressed annealing) or under constant load (Creep).*

Test nature	Test conditions	Density of loops, m^{-3}	Mean diameter, nm
Creep	450°C, 720 h130 MPa	$(6 \pm 1) \times 10^{19}$	139
Unstressed annealing	450°C, 960 h	$(1.2 \pm 1) \times 10^{20}$	176
Creep	400°C, 240 h, 130 MPa	$(1.7 \pm 1) \times 10^{21}$	17
Unstressed annealing	400°C, 250 h	$(2.5 \pm 1) \times 10^{21}$	18
Creep	400°C, 83 h, 250 MPa	5×10^{20}	30

Evolution of Loops During Creep Tests

To analyze the effect of an applied stress on the annealing of loops, several creep tests were performed at various temperatures under various applied stresses. All the creep tests conditions are described in Table 2. The evolution of the loop density, observed by TEM during creep tests, was compared to the pure annealed material. The results are given in Table 8.

The annealing of loops during the creep test performed at 450°C was compared to the unstressed annealing test. The creep test lasted 720 h and the material reached a strain of 7.7 %. As seen previously, the unstressed annealing performed at 450°C lasted 960 h, that is to say, 240 h more than the creep test. The TEM observations, performed on the thermal unstressed annealed material and presented in the first part, revealed that, at this temperature and annealing time, the loops in the unstressed material were almost entirely recovered. Concerning the stressed material, the TEM observations revealed that, like the pure annealed material, a very large part of the density of loops has been annealed. The TEM micrographs, comparing the unstressed annealed microstructure to the crept annealed microstructure, illustrate this result, showing only the presence of large loops of very low density for both materials (Fig. 12). Taking into account the large uncertainties, it can be concluded that no differences can be clearly noticed in the loops size and density between the materials annealed at 450°C without external load or under constant load (130 Mpa).

When creep tests were performed at 400°C under a low applied loading of 130 MPa, no significant difference with pure thermal annealing was observed concerning the loop microstructure (Table 8), as in the previous case. However, the TEM observations performed on the material crept at 400°C under an applied stress of 250 MPa ($\varepsilon = 6$ %), revealed a decrease in the density of loops compared to the 400°C 130 MPa crept material. Moreover, the creep test at 400°C under a load of 250 MPa lasted only 83 h, that is to say, three times less than the 400°C, 130 MPa creep test.

For the material crept at low temperature (350°C), and for a high applied stress of 300 MPa ($\varepsilon = 3.3$ %), the TEM observations revealed the presence of channels in the basal plane (Fig. 13). A channel corresponds to a straight and fine zone, free of loops but surrounded by loops. These zones were formed by the sweeping of the loops caused by the gliding of dislocations. These channels were observed previously after simple burst-test [10].

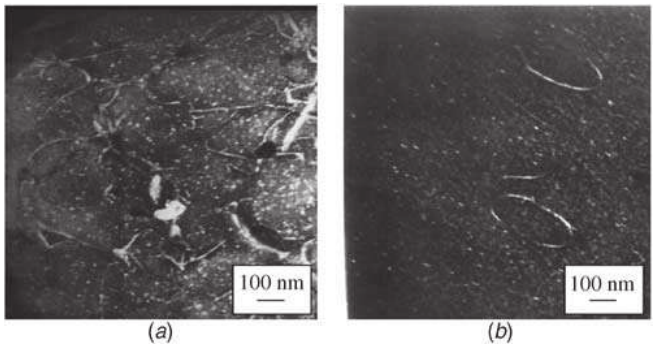

FIG. 12—*Microstructure of loops in (a) 450°C, 130 MPa, 30 days (dark field), and in (b) 450°C, 40 days (dark field).*

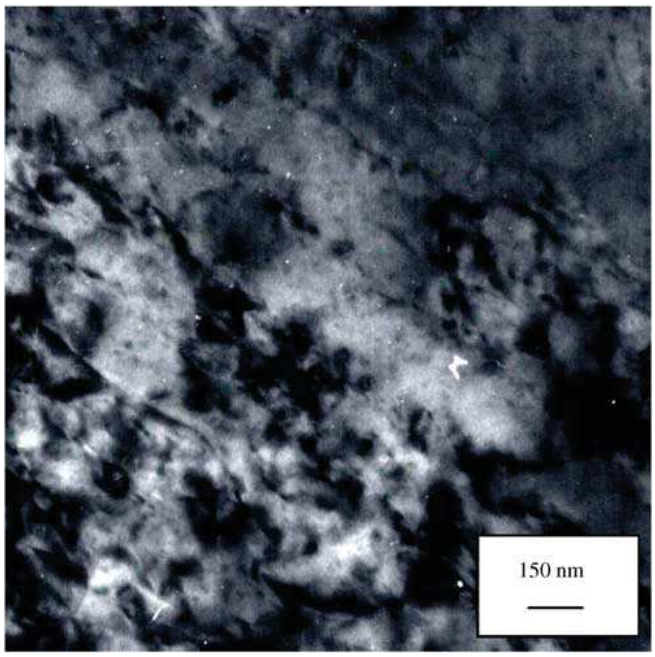

FIG. 13—*Channels in the material crept at 350°C and under 300 MPa (the channels are the clear zone) (bright field) [10].*

Dislocations Evolution During Creep Tests

In order to clarify the effects of the loops on the mobile dislocations, the evolution of the dislocation density with plastic strain during creep testing has been analyzed by TEM in the specimens presented in Table 2. The dislocation density on the irradiated as well as the non-irradiated material in the same loading conditions at the same plastic strain (7.7 % and less than 0.5 % for respectively, 450°C, 130 MPa and 400°C, 130 MPa) has been measured. The TEM observations were focused on the density of dislocations and the nature of activated slip systems. The obtained results are given in Table 9.

The dislocations observed in the irradiated materials tested at 450°C under an applied stress of 130 MPa and the non-irradiated materials tested in the same conditions (Fig. 14) were similar both in terms of slip systems and density. Indeed, all slip systems were activated in both materials.

The evolution of the dislocations at an intermediate temperature (400°C) and low applied stress (130 MPa) also was observed and compared to the non-irradiated material (Fig. 14). First, the dislocation density was 40 times higher (4×10^{14} m^{-2}) in the irradiated sample than in the non-irradiated sample (10^{13} m^{-2}). Secondly, the activated slip systems were different. In the irradiated specimens, due to the loops and dislocations density, it was difficult to determine precisely the Bürgers vector and the glide plane of the dislocations. But, when they were imaged with a diffraction vector $\langle 11\bar{2}0 \rangle$ with the electron beam close to [0002], the dislocations appeared curved. This means that these dislocations belonged to secondary slip systems such as basal or pyramidal slip systems. On the other hand, for the non-irradiated sample, the low dislocations density allowed us to identify easily their Bürgers vector and glide plane. Most of the dislocations glide in the prism plane (P$\langle$a$\rangle$), but some dislocations gliding in the first order pyramidal plane with $\langle$a$\rangle$ Bürgers vector have been found.

A creep test at high applied stress and low temperature, 300 MPa at 350°C was conducted. The previous TEM observations [10] revealed the presence of channels in the basal plane. Consequently, we

TABLE 9—*Slip systems observed in irradiated and non-irradiated Zr-1 %Nb-O specimens.*

Tests conditions	Dislocations density, m^{-2}	Slip systems observed
450°C, 130 MPa, non-irradiated	8×10^{13}	P$\langle$a$\rangle$, $\Pi_1\langle$a$\rangle$, B$\langle$a$\rangle$, $\Pi_1\langle$c+a$\rangle$
450°C, 130 MPa, irradiated	9×10^{13}	P$\langle$a$\rangle$, B$\langle$a$\rangle$, $\Pi_1\langle$c+a$\rangle$
400°C, 130 MPa, irradiated	4×10^{14}	P$\langle$a$\rangle$, $\Pi_1\langle$a$\rangle$, B$\langle$a$\rangle$, $\Pi_1\langle$c+a$\rangle$
400°C, 130 MPa, non-iradiated	10^{13}	P$\langle$a$\rangle$, $\Pi_1\langle$a$\rangle$
350°C, 300 MPa, irradiated	Not measurable	B$\langle$a$\rangle$

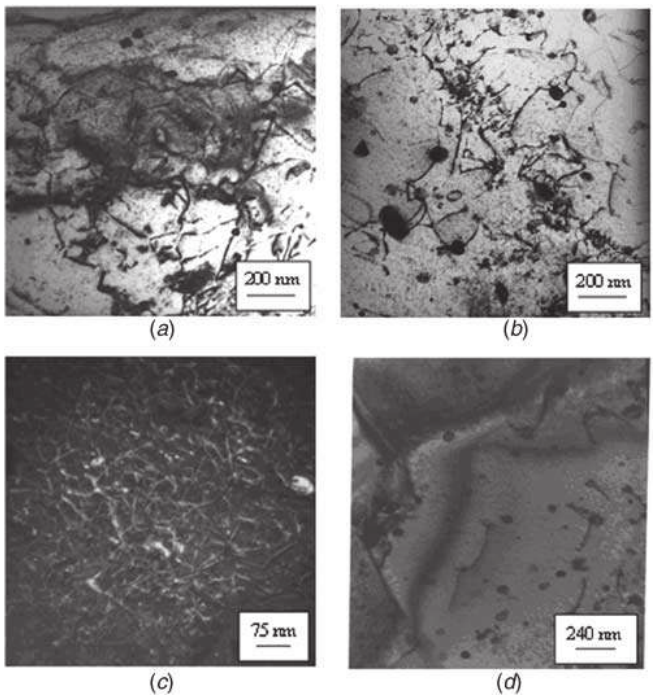

FIG. 14—*Dislocation microstructure comparison between (a) the irradiated (bright field) and (b) the non-irradiated samples (bright field) crept at 450°C, (c) the irradiated (dark field), and (d) the non-irradiated samples (bright field) crept at 400°C.*

conclude that the basal ⟨a⟩ slip systems were activated. No other slip systems were observed, but due to the high dislocation loops density, the observation of dislocations is difficult, the presence of channeling is the only evidence of the dislocation slip.

Discussion

The comparisons of the density of loops established between the materials crept at low applied stress (130 MPa) and at temperature of 400°C and 450°C and the unstrained materials showed that for both temperatures, the same density of loops is present in pure thermal annealed and crept materials. This result means that applied stress has no significant effect on the annealing of loops. Simple thermal annealing of loops occurs during the creep tests and the previous analysis and modeling can be used to predict the microstructure evolution during creep testing. However, this result is only true for an applied stress equal to or below 130 MPa. Indeed, the fact that the density of loops was lower in the material crept at 400°C under an applied stress of 250 MPa than in the material crept at 400°C under an applied stress of 130 MPa, shows that the applied stress played an important role on the disappearance of loops. This phenomenon could be explained by considering that gliding dislocations were able to clear loops during the plastic strain due to the high applied stress. Indeed, it was shown in [4,10] that for internal pressure tests performed at 350°C in simple strain hardening tests basal channeling occurs. The channels are believed to be created by the easy sweeping of loops in the basal plane due to the glissile junctions created between dislocation and loops. This result shows that clearing of loops due to dislocation glide can explain the decrease of the density of loops during creep testing performed at high stress.

It has also been shown that for both tests performed at 450°C on irradiated and the non-irradiated materials, the same microstructures of dislocations in terms of density and slip systems (prism, basal and pyramidal) occur. This result can be explained by the fact that due to the strong thermal annealing of loops at 450°C, the irradiated material becomes similar to the non-irradiated material. The deformation mechanisms are therefore identical. Due to the high temperature test, all the systems are believed to be easily activated in the non-irradiated material according to [35].

The TEM observations performed on the irradiated material crept at 400°C under 130 MPa revealed a high density of dislocations, whereas few dislocations were observed in the non-irradiated sample. This phenomenon can be explained by the fact that the loops act as obstacles and prevent dislocation glide,

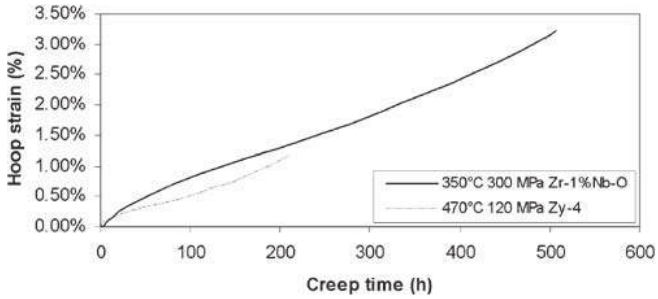

FIG. 15—*Creep test of an irradiated (9×10^{25} n.m^{-2}) stress relieved Zircaloy-4 at 470°C under 120 MPa [38] and creep test of an irradiated (9×10^{25} n.m^{-2}) Zr-1 %Nb-O at 350°C under 300 MPa [10].*

especially in the prism plane. As a consequence a high density of dislocations is needed to deform the material. Indeed, by pinning the dislocations, the loops can act as sources of dislocations that lead to a strong multiplication of dislocations inside the material. This increase of sources of dislocations due to the increase of density of obstacles is discussed for instance in [36]. Furthermore, the dislocations observed probably belong to the second slip systems, basal and pyramidal, which is different from the non-irradiated material where the dislocations essentially belong to prism slip system. This result shows that the loops prevent prism slip system glide and favor the activation of secondary slip systems. This result can be explained by the fact that junctions created between loops and dislocations gliding in prism planes are sessile, whereas they are glissile for dislocations gliding in basal plane. Pyramidal slip also can occur by cross-slip of screw dislocations to overcome loops.

From this analysis, a sequence of events occurring during creep testing for various loading conditions can be proposed. Whatever the applied stress and the test temperature, basal slip occurs first, leading to the clearing of some loops, the prism slip being impeded by sessile junctions. In the case of high applied stress (>200 MPa) and low temperature (350°C), strong basal slip occurs followed by strong clearing of loops. Once the loops have been swept, others slip systems are activated, such as prism and pyramidal slip. However, in the case of low applied stress (<200 MPa) and high temperature (450°C), limited basal slip occurs but rapid thermal annealing of loops. Therefore, slip systems other than basal slip can be activated when loops have disappeared. It can be seen that deformation mechanisms during creep are governed by a competition between clearing of loops (with plastic strain) and thermal annealing of loops (with time assisted by the test temperature).

The proposed deformation mechanisms can explain the mechanical behavior of the irradiated material during creep test described in the literature. Indeed, Yasuda et al. [37] found for Zircaloy-2, at temperatures ranging form 350°C to 425°C and applied stresses ranging from 60 MPa to 190 MPa, that the steady-state creep rate was lower for the irradiated material than for the non-irradiated one. This fact has to be correlated with the present study, which showed that during a creep testing at intermediate temperature and low applied stress (<130 MPa), only low thermal annealing of loops occurs. In consequence, in the study of Yasuda, the creep strength is due to the remaining loops which act as obstacles against glide of dislocations.

For stress relieved Zircaloy-4, Cappelaere et al. [38] observed, that, during a creep test at 470°C and 120 MPa creep acceleration occurs for a low strain (about 0.7 %). Cappelaere et al. attributed this phenomenon to the recovery of loops. Indeed, at this temperature (>450°C) and for this applied stress level (130 MPa), it was shown previously that the recovery of loops is fast and occurs by thermal annealing. This disappearing of loops decreases the creep strength and allows the creep rate of the material to increase, leading to an early accelerated regime (Fig. 15).

Murty et al. [39] found that irradiated zirconium alloy exhibits a more isotropic creep behavior than the non-irradiated material. They attributed this isotropic behavior to the activation of the basal (and pyramidal) systems. Indeed, the present study at intermediate temperature (400°C) also highlighted that the secondary slip systems are strongly activated.

Onimus et al. [10] presented a creep curve from a test at 300 MPa and 350°C on a Zr-1 %Nb-O alloy, where the creep acceleration is visible (Fig. 15). This result means that, despite the low temperature, alloy deformation is possible. Indeed, the TEM observation presented in the present paper revealed that, for

these creep conditions, sweeping of loops occurs. We can conclude in that case that the entry into the accelerated regime of the material is essentially due to the dynamic recovery of loops.

Conclusion

The first part of this paper was devoted to the study of pure thermal annealing of a Zr-1 %Nb-O alloy and a stress relieved Zircaloy-4. The microhardness showed that the material recovers its irradiation microstructure and the TEM observations revealed that the recovery irradiation microstructure occurs by growth of loops and decrease in the density of loops. The main recovery mechanism is believed to be controlled by the exchange of vacancies between loops. The TEM investigations have shown that during the thermal annealing the recovery of interstitial loops was faster than the recovery of vacancy loops.

The second part of this paper based on recovery and glide systems mechanism demonstrated the impact of an applied stress on the recovery of loops of a Zr-1 %Nb-O alloy. Indeed, from TEM observations and for several creep tests performed at different conditions, it was shown that during mechanical loading, annealing could be purely thermal, thermal and dynamic, or purely dynamic. For the low applied stress, the recovery is essentially thermal and its kinetics has thermal-dependent parameters. For a medium temperature test and for a high applied stress, the recovery occurs both through of loops and via thermal recovery, and finally, at low temperature and high applied stresses, the recovery progresses purely through clearing of loops. Furthermore, the TEM observations revealed that the loops act as obstacles to deformation and allow only secondary slip systems to glide.

To sum up, heat treatment, purely thermal or during a creep test, makes the loops disappear from the material, and a sufficiently high applied stress can accelerate this phenomenon.

Acknowledgments

The authors wish to thank AREVA-NP for providing the materials.

References

[1] Jostsons, A., Australian Atomic Energy Commission Report AAEC/E374, 1976.

[2] Northwood, D. O., "Characterization of Neutron Irradiation Damage in Zirconium Alloys—An International "Round-Robin" Experiment," *J. Nucl. Mater.*, Vol. 79, 1979, pp. 379–394.

[3] Lemaignan, C., and Motta, A. T., *Zirconium Alloys in Nuclear Applications, Nuclear Materials*, B.R.T Frost, Ed., Materials Science and Technology Series, Vol. 10B, VCH, New York, R. W. Cahn, P. Haasen, and E. J. Kramer Eds., pp. 1–51.

[4] Onimus, F., Monnet, I., Béchade, J. L., Prioul, C., and Pilvin, P., "A Statistical TEM Investigation of Dislocation Channelling Mechanism in Irradiated Zirconium Alloys," *J. Nucl. Mater.*, Vol. 328, 2004, pp. 165–179.

[5] Howe, L. M., and Thomas, W. R., "The Effects of Neutron Irradiation on the Tensile Properties of Zircaloy-2," *J. Nucl. Mater.*, Vol. 2, No. 3, 1960, pp. 248–260.

[6] Higgy, H. R., and Hammad, F. H., "Effect of Neutron Irradiation on the Tensile Properties of Zircaloy-2 and Zircaloy-4," *J. Nucl. Mater.*, Vol. 44, 1972, pp. 215–227.

[7] Williams, C. D., and Gilbert, R. W., "Radiation Damage in Reactor," *Proc. Syn. Vienna*, IAEA, 1969, pp. 235.

[8] Adamson, R. B., and Bell, W. L., "Effects of Neutron Irradiation and Oxygen Content on the Microstructure and Mechanical Properties of Zircaloy," *Microstructure and Mechanical Behaviour of Materials, International symposium, Xian, China*, October 1985, EMAS, warley, UK, Vol. 1, pp. 237–246.

[9] Eyre, B. L., and Maher, D. M., "Neutron Irradiation Damage in Molybdenum Part V. Mechanisms of Vacancy and Interstitial Loop Growth During Post Irradiation Annealing," *Philos. Mag.*, Vol. 24, 1971, pp. 767–797.

[10] Onimus, F., Béchade, J. L., Prioul, C., Pilvin, P., Monnet, I., Doriot, S., Verhaeghe, B., Gilbon, D., Robert, L., Legras, L., and Mardon, J. P., "Plastic Deformation of Irradiated Zirconium Alloys:

TEM Investigations and Micro-Mechanical Modeling, Zirconium in the Nuclear Industry," *J. ASTM Int.*, Vol. 2, No. 8, 2005, Paper ID JAI12424.
[11] Tenckhoff, E., "Deformation Mechanisms, Texture, and Anisotropy in Zirconium and Zircaloy," ASTM STP 966, ASTM International, West Conshohocken, PA, 1988, pp. 1–77.
[12] Nakatsuka, M., and Nagai, M., "Reduction of Plastic Anisotropy of Zircaloy Cladding by Neutron Irradiation," *J. Nucl. Sci. Technol.*, Vol. 24, 1987, pp. 832–838.
[13] Dunlop, J. W. C., Bréchet, Y. J. M., Legras, L., and Zurob, H. S., "Modeling Isothermal and Non-Isothermal Recrystallisation Kinetics. Application to Zircaloy-4," *J. Nucl. Mater.*, Vol. 366, Nos. 1–2, 2007, pp. 178–186.
[14] Northwood, D. O., "Irradiation Damage in Zirconium and Its Alloys," *At. Energy Rev.*, Vol. 15, No. 4, 1977, pp. 547–610.
[15] Torimaru, T., "Changes in Mechanical Properties of Irradiated Zircaloy-2 Fuel Cladding Due to Short Term Annealing," *J. Nucl. Mater.*, Vol. 238, 1996, pp. 169–174.
[16] Dollins, C. C., "Post Irradiation Recovery of Irradiation Damage," *Radiat. Eff.*, Vol. 16, 1972, pp. 271–280.
[17] Douglass, D. L., *The Metallurgy of Zirconium*, Atomic Energy Review, supplement 1971, IAEA, Vienna, 1971, pp. 277.
[18] Burton, B., and Speight, M. V., "The Coarsening and Annihilation Kinetics of Dislocation Loops," *Philos. Mag. A*, Vol. 53, No. 3, 1986, pp. 385–402.
[19] Kelly, P. M., and Blake, R. G., "The Characterization of Dislocation Loops in Neutron Irradiated Zirconium," *Philos. Mag.*, Vol. 28, 1973, pp. 415–426.
[20] Doriot, S., Gilbon, D., Béchade, J-L., Mathon, M-H., Legras, L., and Mardon, J-P., "Microstructural Stability of M5™ Alloy Irradiated up to High Neutron Fluences," *J. ASTM Int.*, Vol. 2, No. 7, 2005, Paper ID JAI12332.
[21] Maher, D. M., and Eyre, B. L., "Neutron Irradiation Damage in Molybdenum, Part. I Characterization of Small Perfect Dislocation Loops by Transmission Electron Microscopy," *Philos. Mag.*, Vol. 23, 1967, pp. 409–438.
[22] Foreman, A. J. E., "Junction Reaction Hardening by Dislocation Loops," *Philos. Mag.*, Vol. 17, 1968, pp. 353–364.
[23] Hirsch, P. B., Proceedings of a Conference on "*Point Defect Behaviour and Diffusional Processes*" organized by the Metals Society and held at The Royal Fort, University of Bristol, on 13-16 September, 1976, The Metals Society, London, 1977, pp. 95–107.
[24] Nemoto, Y., Hasegawa, A., Satou, M., Abe, K., and Hiraoka, Y., "Microstructural Development and Radiation Hardening of Neutron Irradiated Mo-Re Alloys," *J. Nucl. Mater.*, Vol. 324, 2004, pp. 62–70.
[25] Makin, M. J., Minter, F. J., and Manthorpe, S. A., "The Correlation Between the Crystal Shear Stress of Neutron Irradiated Copper Single Crystals and the Density of Defect Clusters," *Philos. Mag.*, Vol. 13, 1966, pp. 729–739.
[26] Kojima, S., Zinkle, S. J., and Heinisch, H. L., "Radiation Hardening in Neutron-Irradiated Polycrystalline Copper: Barrier Strength of Defect Clusters," *J. Nucl. Mater.*, Vol. 179–181, 1991, pp. 982–985.
[27] Busby, J. T., Hash, M. C., and Was, G. S., "The Relationship Between Hardness and Yield Stress in Irradiated Austenitic and Ferritic Steels," *J. Nucl. Mater.*, Vol. 336, 2005, pp. 267–278.
[28] Northwood, D. O., London, I. M., and Bahen, L. E., "Elastic Constants of Zirconium Alloys," *J. Nucl. Mater.*, Vol. 55, 1975, pp. 299–310.
[29] Moon, J. H., Cantonwine, P. E., Anderson, K. R., Karthikeyan, S., and Mills, M. J., "Characterization and Modeling of Creep Mechanisms in Zircaloy-4," *J. Nucl. Mater.*, Vol. 353, 2006, pp. 177–189.
[30] Derep, J. L., Ibrahim, S., Rouby, R., and Fantozzi, G., "Deformation Behaviour of Zircaloy-4 Between 77 and 900 K," *Acta Metall.*, Vol. 28, 1979, pp. 607–619.
[31] Hardouin Duparc, A., Moingeon, C., Smetniansky-de-Grande, N., and Barbu, A., "Microstructure Modeling of Ferritic Alloys Under High Flux 1 Mev Electron Irradiations," *J. Nucl. Mater.*, Vol. 302, 2002, pp. 143–155.
[32] Christien, F., and Barbu, A., "Effect of Self-Interstitial Diffusion Anisotropy in Electron-Irradiated

Zirconium: A Cluster Dynamics Modeling," *J. Nucl. Mater.*, Vol. 346, 2005, pp. 272–281.

[33] *Atomic Defects in Metals*, Landolt-Börnstein, Vol. 25, H. Ullmaier, Ed., Springer, Berlin, 1991.

[34] Hood, G. M., and Schultz, R. J., "Tracer Diffusion in α-Zr," *Acta Metall.*, Vol. 22, No. 4, 1974, pp. 459–464.

[35] Ferrer, F., Barbu, A., Bretheau, T., Crépin, J., Willaime, F., and Charquet, D., "The Effect of Small Concentrations of Sulfur on the Plasticity of Zirconium Alloys at Intermediate Temperatures," *Zirconium in the Nuclear Industry: Thirteenth International Symposium*, ASTM STP 1423, G. D. Moan, and P. Rudling, eds., ASTM International, West Conshohocken, PA, 2002, pp. 863–887.

[36] Estrin, Y., "Dislocation Theory Based Constitutive Modeling: Foundations and Applications," *J. Mater. Process. Technol.*, Vol. 80–81, 1998, pp. 33–39.

[37] Yasuda, T., and Nakatsuka, M., "Creep Characteristics of Irradiated Zircaloy-2 Cladding Tubes Under Dry Storage Conditions," *Trans. Am. Nucl. Soc.*, Vol. 61, 1990, pp. 77–78.

[38] Cappelaere, C., Limon, R., Gilbon, D., Bredel, T., Rabouille, O., Bouffioux, P., and Mardon, J. P., "Impact of Irradiation Defects Annealing on Long-Term Thermal Creep of Irradiated Zircaloy-4 Cladding Tube," *Zirconium in the Nuclear Industry: Thirteenth International Symposium*, ASTM STP 1423, G. D. Moan, and P. Rudling, eds., ASTM International, West Conshohocken, PA, 2002, pp. 720–739.

[39] Murty, K. L., and Mahmood, S. T., "Effects of Recrystallization and Neutron Irradiation on Creep Anisotropy of Zircaloy Cladding," *Zirconium in the Nuclear Industry: Ninth International Symposium*, ASTM STP 1132, ASTM International, West Conshohocken, 1991, pp. 198–217.